applied sciences

MDPI

Article

Development of a Prolonged-Release Drug Delivery System with Magnolol Loaded in Amino-Functionalized Mesoporous Silica

Alina Stefanache [1], Maria Ignat [2,*], Catalina A. Peptu [3], Alina Diaconu [4], Iulian Stoleriu [5] and Lacramioara Ochiuz [1,*]

1 Faculty of Pharmacy, Grigore. T. Popa University of Medicine and Pharmacy, Iasi 700115, Romania; stef.alina@yahoo.com
2 Faculty of Chemistry, Alexandru Ioan Cuza University of Iasi, Iasi 700560, Romania
3 Faculty of Chemical Engineering and Protection of the Environment, Gheorghe Asachi Technical University of Iasi, Iasi 700050, Romania; catipeptu@ch.tuiasi.ro
4 Petru Poni Institute of Macromolecular Chemistry, Iasi 700487, Romania; alina.diaconu@icmpp.ro
5 Faculty of Mathematics, Alexandru Ioan Cuza University of Iasi, 11 Blvd. Carol I, Iasi 700506, Romania; stoleriu@yahoo.com
* Correspondence: mary_rud@yahoo.com (M.I.); ochiuzd@yahoo.com (L.O.); Tel.: +40-074-650-5227 (M.I.); +40-074-064-8748 (L.O.)

Academic Editors: Yurii K. Gun'ko and Hidenori Otsuka
Received: 14 November 2016; Accepted: 27 February 2017; Published: 2 March 2017

Abstract: Magnolol (MG) is a small-molecule neolignan polyphenolic compound isolated from the genus *Magnolia*. The anti-inflammatory, anti-oxidative, anti-diabetic, anti-tumorgenic, anti-neurodegenerative, anti-depressant and anti-microbial properties of MG are well documented in recent literature. These fascinating multiple biological activities of MG encourage research about the development of new delivery and administration approaches able to maximize its potential benefits. This study describes the amino-functionalization of the SBA-15 (Santa Barbara Amorphous) mesoporous matrix by post-synthesis grafting using APTES (3-aminopropyltriethoxysilane) and the characterization of amino-functionalized mesoporous silica SBA-15 loaded with MG in order to achieve modified drug delivery systems. The amino-functionalization of silica SBA-15 was carried out by grafting by refluxing in dry toluene. The powders obtained were characterized texturally by Brunauer-Emmett-Teller (BET) surface area analysis measurements and morphologically by scanning electron microscopy. MG loading degree in the nanoporous matrix was determined by the HPLC method at λ = 290 nm. Results showed that by grafting the amino groups in the silica SBA-15, we obtained amino-functionalized silica SBA-15 with an ordered structure, with specific surfaces and pore sizes that differ from the original matrix, which was reflected in the amount of MG immobilized and release kinetics profile.

Keywords: magnolol; amino-functionalized; mesoporous silica; prolonged drug; delivery system

1. Introduction

Magnolia officinalis, a species of Magnoliacea, is one of the most popular traditional Chinese medicines. Chinese medicines generally use *Magnolia officinalis* as a remedy for gastrointestinal disorders, acute pain, anxiety, nervous disturbance, diarrhea, cough, phlegm, and a variety of allergic diseases [1–3].

A major bioactive constituent of the bark of *Magnolia officinalis* is 5,5′-diallyl-2,2′-dihydroxybiphenyl, a hydroxylated biphenyl compound called magnolol (MG) whose anti-inflammatory [4], anti-oxidative [5], anti-diabetic, anti-tumorgenic [6], anti-neurodegenerative, anti-depressant and

anti-microbial [7] properties have been recently demonstrated. This compound also regulates hormones, exhibits positive gastrointestinal and uterus modulatory effects, offers cardio-vascular and liver protection and is effective in pain control [8–11].

These fascinating multiple biological activities of magnolol encourage research on the development of new delivery and administration approaches able to maximize its potential benefits. The most popular and convenient administration route for delivering drugs is generally the oral route, but due to significant first-pass metabolism and low absorption, oral bioavailability for magnolol is only 5% [12]. Recent research has demonstrated that nanoencapsulation of bioactive ingredients within a proper matrix leads to the improvement of their therapeutic outcomes when administered orally, by increasing their bioavailability, maximizing their stability in the gastro-intestinal tract through offering protection it from the highly acidic stomach environment, increasing their solubility in the upper gastro-intestinal tract and releasing them sustainably [13].

Numerous current studies focus on the development of new drug delivery systems, based especially on bioactive compounds of natural origin. Such systems are able to deliver the bioactive ingredient at a desired site and time at a specific rate, in accordance with the body particular-treatment necessities. Considerable advances have been lately made on the design of novel drug delivery systems containing plant active ingredients and extracts such as: liposomes, transferosomes, etholsomes phytosomes, nanocapsules, polymeric nano-particles, nanoemulsions, and microspheres. We have not identified in the recent literature any research paper aimed at the formulation of MG in modified-release systems. Most studies concerned with this active molecule are focused on investigating its biological effects [1,14–16].

The development of inorganic delivery systems is aimed at formulating in oral dosage forms, which can improve the bioavailability of the active ingredient and hence its therapeutic outcome [17–22]. The inorganic drug delivery systems containing MG molecules are developed in order to prolong MG release into the human body. For this purpose, in a previous work, the authors of the present paper have proposed mesoporous silica matrix, SBA-15 type, for the encapsulation of magnolol [23] and demonstrated that SBA-15 silica is a compatible matrix for magnolol in formulating sustained-release drug delivery systems. Our previous study has provided scientific results on the textural, structural and morphological properties of magnolol-encapsulated in mesoporous SBA-15 silica, and showed that the hexagonal order of SBA-15 mesopores is conserved after the encapsulation of magnolol.

The effective loading of drug molecules and their subsequent controlled release are facilitated by the unique mesoporous structure of the silica nanoparticles in the form of an ordered pore network, with uniform tunable mesopores that allow close control over drug loading and release kinetics; high pore volume able to host the required amount of pharmaceuticals; high specific surface area with good potential for drug adsorption; and a rich silanol groups-containing surface that can be functionalized to improve control over drug loading and release [24–27].

In such delivery systems, the drug release kinetics is ruled by several factors including the physico-chemical features of the silica surface and the interaction between the carrier and the active molecule. The bioavailability of the silica particles is influenced by characteristics like surface area, zeta-potential, hydrophilicity, functional groups on surface, affinity and selectivity. By altering such particle properties, drug carriers become more effective [28–31].

Silica features can be altered by introducing functional groups on its surface. By now, several studies have already shown that mesoporous silica nanoparticles can be loaded with various bioactive compounds via hydrophobic interactions. Furthermore, SBA-15 functionalized with carboxyl or amino groups demonstrated optimal properties for the release of proteins such as bovine serum albumin due to the balance of electrostatic and hydrophilic interaction between bovine serum albumin and the functionalized SBA-15 matrix [32].

However, when physically adsorbed into the mesoporous structures of silica nanoparticles, the drug molecules may be prematurely released from the carrier, which decreases treatment efficiency and increases potential side-effects [33–37].

The present work uses the results of our previous study and focuses on magnolol loaded in amino-functionalized mesoporous silica. Postsynthesis grafting is the most useful method for functionalizing mesoporous silicas with active groups that are incompatible with the chemistry of the initial sol. Consequently, a desirable thing is to functionalize accessible silica surfaces [38,39], so that postsynthesis grafting involves the silane linkers that are commonly utilized in the bifunctional strategy.

The aim of the present study is to incorporate magnolol into the pores of amino-functionalized mesoporous silica particles. The increase of the magnolol dose loaded in mesoporous silica nanoparticles is aimed at developing solid oral dosage forms with prolonged release.

2. Materials and Methods

2.1. Materials

Tetraethyl orthosilicate (TEOS, 98%) was purchased from Merck KGaA (Darmstadt, Germany). $EO_{20}PO_{70}EO_{20}$ (*Pluronic P123*, 99%) was supplied by Sigma-Aldrich (Aldrich Product No. 435465, Munich, Germany). Hydrochloric acid (32%) was purchased from Chemical Company (Chemical Company S.A., Iasi, Romania). 3-aminopropyltriethoxysilane (APTES, 98%) was purchased from Sigma-Aldrich. Magnolol ≥95% (HPLC), from plant ($C_{18}H_{18}O_2$) was supplied by Sigma-Aldrich (Aldrich Product No. M3445, Munich, Germany). Methanol, chromatographic purity (Merck, Germany); glacial acetic acid chromatographic purity (Merck, Germany); trifluoroacetic acid chromatographic purity (TFA, Merck, Germany); acetonitrile, chromatographic purity (Merck, Germany), potassium phosphate chromatographic purity (Sigma-Aldrich, Germany), and alcohol 99.9% (pro analysis, Sigma-Aldrich, Germany). Deionized water used throughout the experiments was prepared with an ELGA PURELAB Ultra water system. All reagents were used without further purification.

2.2. Methods

2.2.1. SBA-15 Mesoporous Silica Synthesis

In a typical synthesis, 4 g of P123 were dissolved in 30 mL distilled water. In addition, 120 mL of 2 M HCl aqueous solution were added to the clear solution obtained and the resulted mixture was stirred for 2 h at room temperature. Successively, 9.8 mL of TEOS solution were added to the mixture under vigorous stirring for 24 h at 40 °C and then the reaction temperature was raised to 100 °C, for 48 h. The white solid product was recovered by filtration, washed several times with de-ionized water and air-dried at room temperature. In order to remove the surfactant, the white solid product was calcined in air at 550 °C with a heating rate of 1 °C/min and an isothermal period of 6 h [24,25]. The resulted sample was labeled "C".

2.2.2. Modification of the Mesoporous Silica by APTES

The modification of the mesoporous SBA-15 silica with amino groups was accomplished by reacting it with APTES (8 h, 333 K) in toluene. After the reaction, the materials were washed with several portions of toluene, methanol and finally water. In addition, 1 g of the silica was reacted with 5 mL APTES in 30 mL toluene. The SBA-15 sample modified with APTES was labeled "Cf".

2.2.3. Magnolol Immobilization

The magnolol solution and the powdered functionalized or un-functionalized mesoporous silica samples (Cf and C, respectively) were mixed and stirred until equilibrium was achieved. In particular, 200 mg of dried silica material was suspended in 40 mL of 1 mg/mL alcoholic magnolol solution. The suspension was stirred for 2 h and then centrifuged and dried overnight at 50 °C, in order to separate the solid. The resulted product was labeled "C-MG" (magnolol-loaded SBA-15 mesoporous silica) and "Cf-MG" (magnolol-loaded SBA-15 mesoporous silica modified with APTES). The powders

were recovered by centrifugation followed by decantation and filtration. The amount of MG loaded on the silica materials was calculated indirectly by measuring magnolol concentration in the remaining solution by means of HPLC analysis using a liquid chromatograph Thermo Scientific™ UltiMate™ 3000 (Waltham, MA, USA), equipped with a UV-VIS Diode Array Detector. The difference between the concentration of MG in the original solution and in the final solution represents the MG loaded into the matrix.

2.2.4. Quantitative Determination of Magnolol

The chromatographic method applied for the assessment of the loading capacity of silica materials and for the in vitro release tests was developed and validated in-house [40].

The working conditions optimized for the chromatographic system involved the utilization of the mobile phase consisting in a 0.1% TFA in H_2O sol. (solvent A) and methanol (solvent B), in a ratio of 20:80 (v/v), working temperature −30 °C in column TRACER-EXCEL 120 ODS-B (Teknokroma Analytica SA., Catalonia, Spain), 4.6 × 150 mm, 5 µm, injection of a sample volume of 20 µL and chromatogram recording at a wavelength of 290 nm. The method was validated by determining the following parameters: method *repeatability* and *intermediate precision* for a concentration of 0.5 mg/mL, when we obtained RSD (Relative Standard Deviation) values ≤ 2.5 for peak area, retention time and concentration; method linearity in the concentration range of 0.025–1.5 mg/mL, equation of curve calibration $y = 492.05x + 6.5518$) ($R^2 = 0.9985$); detection limit—0.00988 mg/mL and quantification limit—0.02993 mg/mL; method robustness was determined by injecting MG solutions (concentrations 0.5 and 1 mg/mL) under various flow and temperature conditions.

2.2.5. Characterization Methods of MG-Loaded Mesoporous Silica

Nitrogen Sorption Isotherms

The nitrogen sorption isotherms were recorded on a Quantachrome Nova 2200 Instrument and Pore Size Surface Area Analyzer (Quantachrome Instruments, Odelzhausen, Germany) at −196 °C. Before measurements, the samples were outgassed under high vacuum at room temperature for 12 h. The Brunauer-Emmett-Teller (BET) specific surface area (S_{BET} (m^2/g)) was calculated from the linear part of the BET plot. Micropore area (S_μ (m^2/g)) was determined by a *t*-plot method. The average pore diameter (D_p (nm)) was estimated using the desorption branch of the isotherm and the Barrett-Joyner-Halenda (BJH) model [29,41]. The volume of liquid nitrogen adsorbed $P/P_0 = 0.95$ was used to assess the total pore volume (TPV (cm^3/g)).

Scanning Electron Microscopy (SEM)

The Scanning Electron Microscopy (SEM) investigations were performed using a Vega Tescan electron microscope (Tescan Orsay Holding, Brno, Czech Republic).

Fourier Transform Infrared Spectroscopy (FTIR)

The FTIR spectra were collected on a Vertex 70 (Bruker Co., Billerica, MA, USA) using a KBr pellet technique. The KBr pellets were prepared by mixing 3 mg of silica sample with 500 mg spectroscopy grade KBr. Spectra were recorded on all formulations as well as on raw materials (C, C-MG, Cf, Cf-MG, MG). The spectra obtained were compared with those reported in the literature.

2.2.6. In Vitro Dissolution Tests

In vitro dissolution tests were performed using an SR 8 Plus Series (ABL & E Jasco Co., Cluj-Napoca, Romania) device, according to the following experimental protocol: drug sample: 150 mg of free unencapsulated MG, 2.727 g C-MG, and 1.200 g Cf-MG. Matrix mass was calculated based on the loading degree of each matrix, so that a concentration of 0.3 mg MG/mL corresponds to a 100% dissolution of MG; dissolution medium: 500 mL of simulated gastric fluid (pH 1.2, HCl 0.1 N)

for the first 2 h and 500 mL simulated intestinal fluid (pH 6.8—phosphate buffer) for the next 22 h; Apparatus 2 (paddles); bath temperature 37 °C ± 0.5 °C; rotation speed: 50 rpm; and sampling time was set to an hour for 24 h. Furthermore, 3 mL of sample was retrieved every hour and concurrently replaced with the same volume of medium. The quantitative determination of MG was performed by an HPLC method developed in-house, as previously described. All dissolution tests were made in triplicate, with the mean values reported in the graphics/diagrams/tables (relative standard deviation, RSD < 5%).

2.2.7. Analysis of In Vitro Drug Release Kinetics

In order to predict and correlate the behavior of the in vitro MG release from the mesoporous silica, a suitable mathematical model was used. Thus, the experimental data obtained from the in vitro dissolution tests were investigated using five predictable models: zero-order and first-order kinetics, Higuchi, Korsmeyer-Peppas and sigmoidal models [42–45]. Data fitting was performed by linear and nonlinear regression using Matlab 7.1. (MathWorks, Natick, MA, USA). Data were presented as mean ± standard deviation and were considered statistically significant at $p < 0.05$. The Akaike information criterion (AIC) and the correlation coefficient R^2 were the criteria for selecting the model that most dependably describes the release profile of each formula. In a reliable prediction model, the value of R^2 is as close to 1 as possible, and AIC has the lowest values possible [46,47].

3. Results

3.1. Magnolol Loading Capacity

Adsorption capacity (the maximum adsorbed amount of analyte on 1.0 g sorbent) is an important factor in the evaluation of a sorbent. The final concentration of MG in the post-loading solution was 0.725 mg/mL for sample C-MG and 0.375 mg/mL sample Cf-MG. Subsequently, the calculated adsorption efficiency values were 55 mg/g of for the un-functionalized silica and 125 mg/g for the APTES-modified silica nanoparticles, respectively. The results show that by functionalization the capacity of mesoporous SBA-15 silica to load MG increased by 227%.

3.2. Characterization of MG-Loaded Mesoporous Silica

3.2.1. Textural Properties

The textural properties of the obtained silica systems were characterized by N_2-sorption measurements. The uptake and release of drug molecules generally depend on the specific surface area, total pore volume and pore diameter of the mesoporous silica materials [27,30,41]. Basically, the reason for using such measurements is to investigate any modification of the textural properties of the porous silica material. Figure 1a,b shows the recorded isotherms and the corresponding pore size distribution curves for the necked mesoporous SBA-15 silica (C), APTES-functionalized mesoporous SBA-15 silica (Cf), and magnolol-loaded APTES-functionalized mesoporous SBA-15 silica material (Cf-MG).

According to the International Union of Pure and Applied Chemistry (IUPAC) classification, all four adsorption-desorption isotherms are of type IV, with a well-defined capillary condensation stage in which the relative pressure of 0.6–0.8 occurs, and a steep hysteresis loop characteristic to mesoporous materials with pore sizes of 7–8 nm. It is easy to observe that functionalization has influenced both the specific surface area and pore diameter. The presence of magnolol molecules in the SBA-15 cylindrical pores is proved by the decrease of the adsorbed nitrogen volume, of the total pore volume and of the specific surface area.

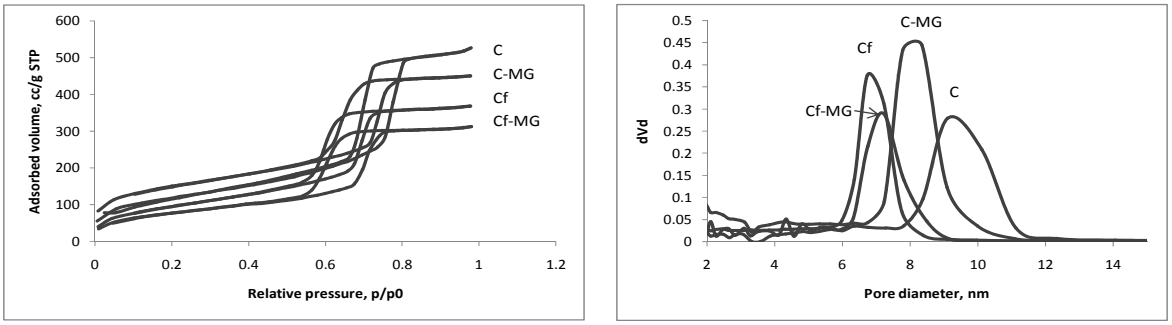

(**a**) (**b**)

Figure 1. (**a**) N_2 adsorption-desorption isotherms; (**b**) corresponding Barrett-Joyner-Halenda (BJH) pore size distribution curves of mesoporous SBA-15 silica (C), APTES (3-aminopropyltriethoxysilane)-functionalized mesoporous SBA-15 silica (Cf), and magnolol-loaded APTES-functionalized mesoporous SBA-15 silica material (Cf-MG).

As can be seen, APTES and magnolol do not actually introduce a marked change in the shape of the isotherm or of the hysteresis loop. The functionalization step and the further loading of magnolol conduct for the pore narrowing noted in the pore size distribution patterns.

The pore size distribution curves report on pore size homogeneity and are used for evaluating the diameters of the pores by applying the BJH model. Figure 1a shows that all porous systems are characterized by a narrow pore size distribution, with the mean pore diameter of 8.3 for the necked SBA-15 silica and only 7.2 nm for the functionalized magnolol-loaded silica. As expected, 65% of the specific surface area was lost in the case of magnolol-loaded APTES-functionalized mesoporous SBA-15 silica material, while, with the APTES-functionalized mesoporous SBA-15 silica, the loss is 55% and for the magnolol-loaded unfunctionalized silica C-MG, 47%. A 47% reduction of the total pore volume occurred for sample Cf and 55% for the Cf-MG system, while, in the case of sample C-MG, the reduction was of about 25% only. All calculated textural features are presented in Table 1.

Table 1. Textural properties of the prepared silica-based systems.

Sample	Specific Surface Area S_{BET} (m^2/g)	% Loss of S_{BET}	Pore Volume V_{pore} (cc/g)	% Loss of V_{pore}	Pore Diameter D_{pore} (nm)	Micropore Surface S_{μ} (m^2/g)	% Porosity
C	794.65	100	1.071	100	10	214.1	70
C-MG	412.99	47	0.802	25	8.3	12.7	63
Cf	349.43	55	0.566	47	6.7	0	55
Cf-MG	275.32	65	0.478	55	7.2	10.9	51

S_{BET}: Brunauer-Emmett-Teller Surface Area Analysis.

3.2.2. Morphological Properties

The morphology of the silica particles has an impact on their drug loading and release capacity. Particle size and shape of the prepared materials were investigated using SEM technique and are shown in Figure 2. SEM images of SBA-15 silica (C sample) and magnolol-loaded silica (C-MG) show a fiber-like morphology of the particles at large scale and a worm-like shape of the particles at small scale. When the silica is modified with APTES, the matrix loses its fiber-like morphology on a large scale and particle agglomeration occurs [48–50].

No similar change occurs with the worm-like shapes on a small scale.

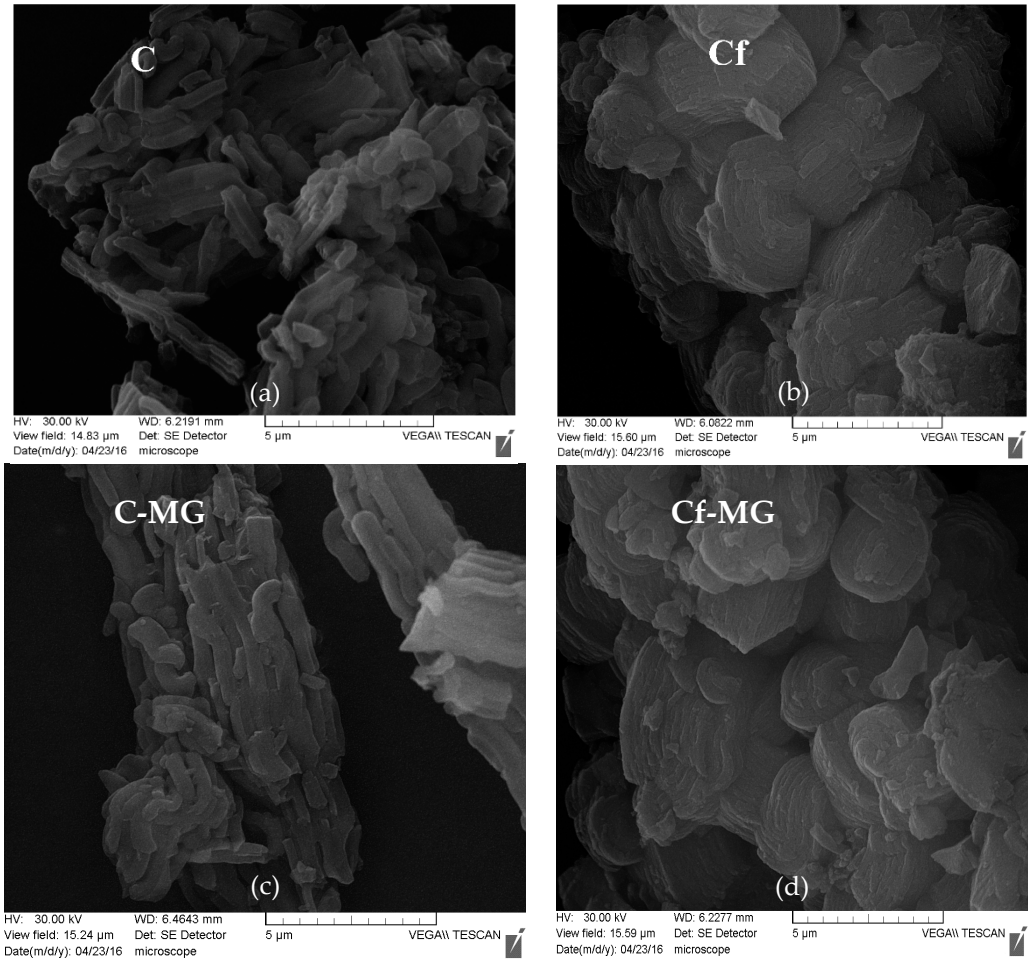

Figure 2. SEM images for: (**a**) pure SBA-15 silica (C); (**b**) functionalized SBA-15 silica with APTES (Cf); (**c**) magnolol loaded in SBA-15 silica (C-MG) and (**d**) magnolol loaded in functionalized SBA-15 silica with APTES (Cf-MG).

3.2.3. Fourier Transform Infrared Spectroscopy (FTIR)

The formation of magnolol-loaded silica composites is demonstrated by FTIR spectroscopy. Figure 3 shows the FTIR spectra of bare SBA-15 silica and silica with modified surface (APTES, MG, APTES/MG). The absorption spectrum of MG shows absorption bands in the range 3340–2663, 1649–1015 and 997–418 cm^{-1} [51].

As the MG curve shows, the intense absorption band attributed to the hydroxyl stretching vibration occurs at 3138 cm^{-1}. The presence of allyl C=C stretching vibration is determined by the absorption band at 1637 cm^{-1}, while C=C aromatic stretching is characterized by the 1494 cm^{-1} absorption band. The broad peak in the range 3340–2663 cm^{-1} includes the stretching vibration of aliphatic C–H, C–O and Ar-H bending vibration.

The FTIR spectra of the pure, functionalized and MG-loaded silica show an intense broad absorption band at 3600–3200 cm^{-1} corresponding to the free –OH stretches vibration. This wide absorption peak and the vibration of Si–OH groups overlap, the entire broad peak of the area being generally attributed to the influence of the hydrogen bonds. In the curves of functionalized and magnolol-loaded silica samples, the peak is lightly modified because the functionalization process and magnolol molecules block active sites and leave smaller amounts of free Si–OH groups on the silica surface. This is an indication that the silica surface has been successfully functionalized with

APTES molecules, and/or further grafted with magnolol species evidenced by the shoulder close to 3200 cm^{-1} wavenumber. At wave values >1240 cm^{-1}, no modification is identified. [52].

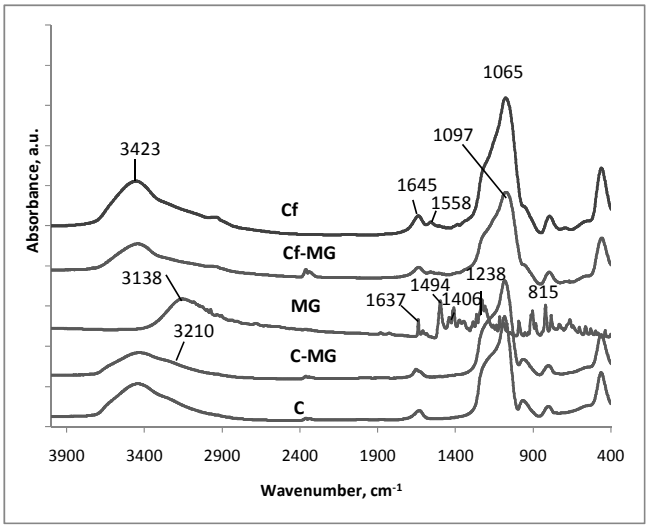

Figure 3. Comparative representation of Fourier Transform Infrared Spectroscopy (FTIR) spectra recorded.

The grafting of $–NH_2$ groups on the pore wall surface is proved by the IR band at 1645 cm^{-1} with a lower intensity shoulder at 1558 cm^{-1}. The bands are assigned to the asymmetric and symmetric deformation modes of the $–NH_2$ groups fixed on the silica surface. [53].

3.3. In Vitro Release of MG-Loaded Mesoporous Silica and Analysis of MG Release Kinetics

In vitro dissolution tests revealed a prolonged release of MG from both functionalized and un-functionalized mesoporous silica, compared to the dissolution profile of unloaded MG (Figure 4).

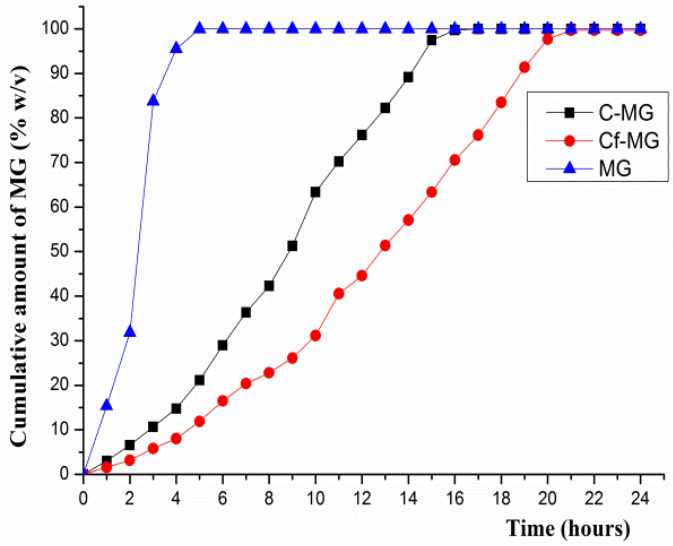

Figure 4. In vitro dissolution release of MG form mesoporous silica.

Furthermore, study results have shown that the capacity for extended release of silica is enhanced by functionalization. Thus, in the first 10 h of the test, Cf-MG released 31.16% of the MG loaded, while the C-MG unfunctionalized matrix caused a release of 63.36%. Thus, the un-functionalized matrix

achieved a prolonged release of MG over 15 h, whereas the functionalized SBA-15 showed capabilities for retardation of release covering over 20 h. These results are consistent with other published results that evidenced an increase in the drug loading capacity of SBA-15 silica. It is important to note that the rate of drug release decreases proportionally with the increase of the loading capacity due to the electrostatic interactions that occur between the functional groups and the drug molecule [23,41]. These results are additionally confirmed by the release kinetics analysis of the mesoporous silica (Table 2). The sigmoid-shaped drug delivery model best defines the release of MG from both C-MG and Cf-MG. Basically, the release rate of MG presents three phases, with a slow first phase which is more pronounced for Cf-MG because the amine groups of SBA-15 interact with the hydroxyl groups in the structure of MG (Figure 5) [54].

Table 2. Results of curve fitting of the in vitro release profile of magnolol (MG) from mesoporous silica SBA-15.

Kinetic Model	Model Coefficients	Mesoporous Silica	
		C-MG	Cf-MG
Zero-order	K_0	5.2110	4.3009
	R^2	0.9068	0.9563
	AIC	119.7224	99.7687
First-order	K_1	0.3389	0.1586
	R^2	0.2499	0.2584
	AIC	169.7668	167.7206
Higuchi	K_H	20.8929	16.6807
	R^2	0.8462	0.7343
	AIC	131.7288	143.0910
Korsmeyer-Peppas	n	0.90	0.98
	K_P	6.9464	4.5512
	R^2	0.9230	0.9524
	AIC	117.1378	103.8153
Sigmoidal	M	28.7	42.9
	K	0.39	0.3
	R^2	0.9963	0.9911
	AIC	44.2082	63.7028

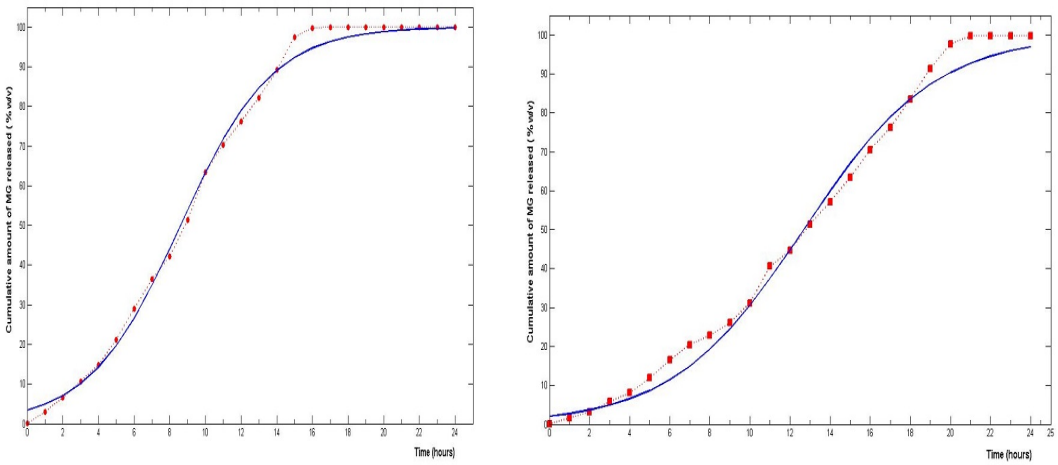

(**a**) (**b**)

Figure 5. Sigmoidal plot of MG release from C-MG (**a**) and Cf-MG (**b**).

The second time-dependent stage of MG release has a duration of 15 h for the Cf-MG matrix and only 7–8 h for C-MG. The third phase of MG release begins once the steady-state concentration is reached, and eventually reveals the release of 100% of the MG loaded in the matrix.

4. Conclusions

The study describes the modification of SBA-15 silica surface for the loading of magnolol bioactive molecules. Experimental outcomes demonstrated that APTES-modified SBA-15 silica nanoparticles are able to uptake a higher amount of magnolol on their surface. The loading capacity of the functionalized silica sample was compared to a non-functionalized silica sample, and it was found to be 2.5 times higher. The efficient uptake of magnolol was also confirmed by BET measurements, which allowed the calculation of the textural properties of the synthesized materials by means of BET specific surface area, total pore volume and pore diameter. It was demonstrated that the process of amino-functionalization of silica material leads to an enhanced MG delivery system with a prolonged release profile fitted on a sigmoidal model. APTES-functionalization proved the loss of the morphological properties of silica nanoparticles on a large scale, while the worm-like morphology of the silica particles on a small scale remained unchanged. A subsequent study using various levels of amino-functionalization of SBA-15 silica powder is in progress and will be reported in separate research work.

Acknowledgments: This research was financed by the Grigore T. Popa University of Medicine and Pharmacy Iasi, Romania, and belongs to the Internal Research Program: Project No. 30889/2014.

Author Contributions: Alina Stefanache, Maria Ignat and Lacramioara Ochiuz conceived and designed the experiments. They were involved in the textural and morphological assessment of samples. Catalina A. Peptu performed the FTIR measurements. Alina Diaconu made the determination of specific surfaces of pores and Iulian Stoleriu has made the fitation by mathematics methods. All authors have contributed equally to this work.

Conflicts of Interest: The authors declare no conflict of interest.

References

1. Liu, Y.; Cao, W.; Zhang, B.; Liu, Y.; Wang, Z.; Wu, Z.; Yu, X.; Zhang, X.; Ming, P.; Zhou, G.; Huang, L. The natural compound magnolol inhibits invasion and exhibits potential in human breast cancer therapy. *Sci. Rep.* **2013**, *3*, 3098. [CrossRef] [PubMed]
2. Shen, J.L.; Man, K.M.; Huang, P.H.; Chen, W.C.; Chen, D.C.; Cheng, Y.W.; Liu, P.L.; Chou, M.C.; Chen, Y.H. Honokiol and magnolol as multifunctional antioxidative molecules for dermatologic disorders. *Molecules* **2010**, *15*, 6452–6465. [CrossRef] [PubMed]
3. Chen, Y.H.; Huang, P.H.; Lin, F.Y.; Chen, W.C.; Chen, Y.L.; Yin, W.H.; Man, K.M.; Liu, P.L. Magnolol: A multifunctional compound isolated from the Chinese medicinal plant *Magnolia officinalis*. *Eur. J. Integr. Med.* **2011**, *3*, 317–324. [CrossRef]
4. Lee, J.; Jung, E.; Park, J.; Jung, K.; Lee, S.; Hong, S.; Park, J.; Park, E.; Kim, J.; Park, S.; et al. Anti-inflammatory effects of magnolol and honokiol are mediated through inhibition of the downstream pathway of MEKK-1 in NF-kappab activation signaling. *Planta Med.* **2005**, *71*, 338–343. [CrossRef] [PubMed]
5. Pang, Y.L.; Han, X.F.; Bamiloye, M.A.; Gong, Z.H.; Tang, S.X.; Tan, Z.L.; Xiao, W.J.; Zhou, C.S.; Wang, M.; Deng, Y.L. Anti-diarrhea and anti-oxidant properties of Magnolol. *Trop. J. Pharm. Res.* **2013**, *12*, 85–91. [CrossRef]
6. Ikeda, K.; Sakai, Y.; Nagase, H. Inhibitory effect of magnolol on tumour metastasis in mice. *Phytother. Res.* **2003**, *17*, 933–937. [CrossRef] [PubMed]
7. Ho, K.Y.; Tsai, C.C.; Chen, C.P.; Huang, J.S.; Lin, C.C. Antimicrobial activity of honokiol and magnolol isolated from *Magnolia officinalis*. *Phytother. Res.* **2001**, *15*, 139–141. [CrossRef] [PubMed]
8. Matsui, N.; Takahashi, K.; Takeichi, M.; Kuroshita, T.; Noguchi, K.; Yamazaki, K.; Tagashira, H.; Tsutsui, K.; Okada, H.; Kido, Y.; et al. Magnolol and honokiol prevent learning and memory impairment and cholinergic deficit in SAMP8 mice. *Brain Res.* **2009**, *1305*, 108–117. [CrossRef] [PubMed]
9. Lin, Y.R.; Chen, H.H.; Lin, Y.C.; Ko, C.H.; Chan, M.H. Antinociceptive actions of honokiol and magnolol on glutamatergic and inflammatory pain. *J. Biomed. Sci. Eng.* **2009**, *16*, 94. [CrossRef] [PubMed]

10. Lu, Y.C.; Chen, H.H.; Ko, C.H.; Lin, Y.R.; Chan, M.H. The mechanism of honokiol-induced and magnolol-induced inhibition on muscle contraction and Ca^{2+} mobilization in rat uterus. *Naunyn Schmiedeberg's Arch. Pharmacol.* **2003**, *368*, 262–269. [CrossRef] [PubMed]
11. Zhang, W.W.; Li, Y.; Wang, X.Q.; Tian, F.; Cao, H.; Wang, M.W.; Sun, Q.S. Effects of magnolol and honokiol derived from traditional Chinese herbal remedies on gastrointestinal movement. *World J. Gastroenterol.* **2005**, *11*, 4414–4418. [CrossRef] [PubMed]
12. Tsai, T.H.; Chou, C.J.; Lee, T.F.; Wang, L.C.H.; Chen, C.F. Pharmacokinetic and pharmacodynamic studies of magnolol after oral administration in rats. *Pharm. Pharmacol. Commun.* **1996**, *2*, 191–193.
13. Ajazuddin; Saraf, S. Applications of novel drug delivery system for herbal formulations. *Fitoterapia* **2010**, *81*, 680–689. [CrossRef] [PubMed]
14. Chiu, J.H.; Wang, J.C.; Lui, W.Y.; Wu, C.W.; Hong, C.Y. Effect of magnolol on in vitro mitochondrial lipid peroxidation and solated cold-preserved warm-reperfused rat livers. *J. Surg. Res.* **1999**, *82*, 11–16. [CrossRef] [PubMed]
15. Li, H.B.; Gao, J.M.; Ying, X.X.; Wang, S.P.; Li, J.C. Protective effect of magnolol on TBHPinduced injury in H460 cells partially via a p53 dependent mechanism. *Arch. Pharm. Res.* **2007**, *30*, 850–857. [CrossRef] [PubMed]
16. Dikalov, S.; Losik, T.; Arbiser, J.L. Honokiol is a potent scavenger of superoxide and peroxyl radicals. *Biochem. Pharmacol.* **2008**, *76*, 589–596. [CrossRef] [PubMed]
17. Takata, T.; Tsunoji, N.; Takamitsu, Y.; Sadakane, M.; Sano, T. Nanosized CHA zeolites with high thermal and hydrothermal stability derived from the hydrothermal conversion of FAU zeolite. *Microporous Mesoporous Mater.* **2016**, *225*, 524–533. [CrossRef]
18. Newalkar, B.L.; Choudary, N.V.; Kumar, P.; Komarneni, S.; Bhat, T.S.G. Exploring the potential of mesoporous silica, SBA-15, as an adsorbent for light hydrocarbon separation. *Chem. Mater.* **2002**, *14*, 304–309. [CrossRef]
19. Benamor, T.; Vidal, M.L.; Lebeau, B.; Marichal, C. Influence of synthesis parameters on the physico-chemical characteristics of SBA-15 type ordered mesoporous silica. *Microporous Mesoporous Mater.* **2012**, *153*, 100–114. [CrossRef]
20. Wang, Z.; Zhao, Q.; Han, N.; Ling, B.; Liu, J.; Liang, H.; Zhang, Q.; Jiang, T.; Wang, S. Mesoporous silica nanoparticles in drug delivery and biomedical applications. *Nanomed. Nanotechnol.* **2015**, *11*, 313–327. [CrossRef] [PubMed]
21. Zhang, J.; Yuan, Z.F.; Wang, Y.; Chen, W.H.; Luo, G.F.; Cheng, S.X.; Zhuo, X.R.; Zhang, X.Z. Multifunctional envelope-typemesoporous silica nanoparticles for tumortriggered targeting drug delivery. *J. Am.Chem. Soc.* **2013**, *135*, 5068–5073. [CrossRef] [PubMed]
22. Chen, Z.; Li, Z.; Lin, Y.; Yin, M.; Ren, J.; Qu, X. Bioresponsive hyaluronic acid-capped mesoporous silica nanoparticles for targeted drug delivery. *Chem. Eur. J.* **2013**, *19*, 1778–1783. [CrossRef] [PubMed]
23. Stefanache, A.; Tomoiaga, A.M.; Peptu, C.A.; Spac, A.; Ochiuz, L. Development of prolonged-release systems with magnolol based on silica SBA-15. In Proceedings of the 15th International Multidisciplinary Scientific GeoConference, Albena, Bulgaria, 18–24 June 2015; Book 6. Volume 1, pp. 53–67.
24. Vallet-Regi, M.; Balas, F.; Arcos, D. Mesoporous Materials for Drug Delivery. *Angew. Chem. Int. Ed.* **2007**, *46*, 7548–7558. [CrossRef] [PubMed]
25. Piao, Y.; Burns, A.; Kim, J.; Wiesner, U.; Hyeon, T. Designed fabrication of silica-based nanostructured particle systems for nanomedicine applications. *Adv. Funct. Mater.* **2008**, *18*, 3745–3758. [CrossRef]
26. Huang, X.; Li, L.; Liu, T.; Hao, N.; Liu, H.; Chen, D.; Tang, F. The shape effect of mesoporous silica nanoparticles on biodistribution, clearance, and biocompatibility in vivo. *ACS Nano* **2011**, *5*, 5390–5399. [CrossRef] [PubMed]
27. Wang, Y.; Zhao, Q.; Hu, Y.; Sun, L.; Bai, L.; Jiang, T.; Wang, S. Ordered nanoporous silica as carriers for improved delivery of water insoluble drugs: A comparative study between three dimensional and two dimensional macroporous silica. *Int. J. Nanomed.* **2013**, *8*, 4015–4031. [CrossRef] [PubMed]
28. Owens, D.E.; Peppas, N.A. Opsonization, biodistribution, and pharmacokinetics of polymeric nanoparticles. *Int. J. Pharm.* **2006**, *307*, 93–102. [CrossRef] [PubMed]
29. Zhou, Z.; Zhu, S.; Zhang, D. Grafting of thermo-responsive polymer inside mesoporous silica with large pore size using ATRP and investigation of its use in drug release. *J. Mater. Chem.* **2007**, *17*, 2428–2433. [CrossRef]
30. Yang, P.; Gai, S.; Lin, J. Functionalized mesoporous silica materials for controlled drug delivery. *Chem. Soc. Rev.* **2012**, *41*, 3679–3698. [CrossRef] [PubMed]

31. Hu, Y.; Zhi, Z.; Zhao, Q.; Wu, C.; Zhao, P.; Jiang, H.; Jiang, T.; Wang, S. 3D cubic mesoporous silica microsphere as a carrier for poorly soluble drug carvedilol. *Microporous Mesoporous Mater.* **2012**, *147*, 94–101. [CrossRef]
32. Song, S.W.; Hidajat, K.; Kawi, S. Functionalized SBA-15 Materials as Carriers for Controlled Drug Delivery: Influence of Surface Properties on Matrix-Drug Interactions. *Langmuir* **2005**, *21*, 9568–9575. [CrossRef] [PubMed]
33. Hayashi, K.; Nakamura, M.; Ishimura, K. Silica-porphyrin hybrid nanotubes for in vivo cell tracking by near-infrared fluorescence imaging. *Chem. Commun.* **2012**, *48*, 3830–3832. [CrossRef] [PubMed]
34. Gao, W.; Chan, J.M.; Farokhzad, O.C. pH-responsive nanoparticles for drug delivery. *Mol. Pharm.* **2010**, *7*, 1913–1920. [CrossRef] [PubMed]
35. Qu, F.; Zhu, G.; Lin, H.; Zhang, W.; Sun, J.; Li, S.; Qiu, S. A controlled release of ibuprofen by systematically tailoring the morphology of mesoporous silica materials. *J. Solid State Chem.* **2006**, *179*, 2027–2035. [CrossRef]
36. Carriazo, D.; Del Arco, M.; Fernández, A.; Martín, C.; Rives, V. Inclusion and release of fenbufen in mesoporous silica. *J. Pharm. Sci.* **2010**, *99*, 3372–3380. [CrossRef] [PubMed]
37. Ashley, C.E.; Carlee, E.; Carnes, E.C.; Phillips, G.K.; Padilla, D.; Durfee, P.N.; Brown, P.A.; Hanna, T.N.; Liu, J.W.; Phillips, B.; et al. The targeted delivery of multicomponent cargos to cancer cells by nanoporous particle-supported lipid bilayers. *Nat. Mater.* **2011**, *10*, 389–397. [CrossRef] [PubMed]
38. He, Q.; Zhang, Z.; Gao, F.; Li, Y.; Shi, J. In vivo biodistribution and urinary excretion of mesoporous silica nanoparticles: Effects of particle size and PEGylation. *Small* **2011**, *7*, 271–280. [CrossRef] [PubMed]
39. Trewyn, B.G.; Slowing, I.; Giri, S.; Chen, H.T.; Lin, V.S.Y. Synthesis and functionalization of a mesoporous silica nanoparticle based on the sol-gel process and applications in controlled release. *Acc. Chem. Res.* **2007**, *40*, 846–853. [CrossRef] [PubMed]
40. Stefanache, A.; Ochiuz, L.; Ignat, M.; Creteanu, A.; Tantaru, G. Development and Validation of a New Method by High-Performance Liquid Chromatography for the Quantitative Analysis of Magnolol Loaded in Silica Particulate Systems. *Farmacia* **2016**, *64*, 268–273.
41. Chakraborty, I.; Mascharak, P.K. Mesoporous silica materials and nanoparticles as carriers for controlled and site-specific delivery of gaseous signaling molecules. *Microporous Mesoporous Mater.* **2016**, *234*, 409–419. [CrossRef]
42. Costa, P.; Sousa, I.; Lobo, J.M. Modeling and comparison of dissolution profiles. *Eur. J. Pharm. Sci.* **2001**, *13*, 123–133. [CrossRef]
43. Siepman, J.; Gopferich, A. Mathematical modeling of bioerodable, polymeric drug delivery systems. *Adv. Drug Deliv. Rev.* **2001**, *48*, 229–242. [CrossRef]
44. Mahat, B.S. Mathematical Models used in the Drug Release Studies. Submitted for internal evaluation for the degree in master in Pharmacy, Kathmandu University, Dhulikhel, Nepal, 2010; pp. 1–26.
45. Losi, E.; Bettini, R.; Santi, P.; Sonvico, F.; Colombo, G.; Lofthus, K.; Colombo, P.; Peppas, N.A. Assemblage of novel release modules for the development of adaptable drug delivery systems. *J. Control. Release* **2006**, *111*, 212–218. [CrossRef] [PubMed]
46. Gohel, M.C.; Sarvaiya, K.G.; Shah, A.R.; Brahmbhatt, B.K. Mathematical approach for the assessment of similarity factor using a new scheme for calculating weight. *Indian J. Pharm. Sci.* **2009**, *71*, 142–144. [CrossRef] [PubMed]
47. Wang, Y.; Sun, L.; Jiang, T.; Zhang, J.; Zhang, C.; Sun, C.; Denq, Y.; Sun, J.; Wang, S. The investigation of MCM-48-type and MCM-41-type mesoporous silica as oral solid dispersion carriers for water insoluble cilostazol. *Drug. Dev. Ind. Pharm.* **2014**, *40*, 819–828. [CrossRef] [PubMed]
48. Enrichi, F.; Trave, E.; Bersani, M. Acid synthesis of luminescent amine functionalized or erbium-doped silica spheres for biological applications. *J. Fluoresc.* **2008**, *18*, 507–511. [CrossRef] [PubMed]
49. Amanpreet, S.; Manchanda, M.K. Synthesis of large-pore face-centered-cubic periodic mesoporous organosilicas with unsaturated bridging groups. *Microporous Mesoporous Mater.* **2016**, *222*, 153–159.
50. Majda, D.; Makowski, W.M.; Mańko, K.; Mlekodaj, A.; Michalik-Zym, A.; Napruszewska, B.D.; Zimowska, M.; Serwicka, E.M. Porosity characterization of SBA-15 silicas with thermoporosimetry of water and *n*-alkanes—The effect of the probe liquid nature. *Microporous Mesoporous Mater.* **2015**, *201*, 141–150. [CrossRef]

51. Qiu, N.; Shen, B.; Li, X.; Zhang, X.; Sang, Z.; Yang, T.; An, L.; Liu, J.; Chen, L.; Wang, L. Inclusion complex of magnolol with hydroxypropyl-β-cyclodextrin: Characterization, solubility, stability and cell viability. *J. Incl. Phenom. Macrocycl. Chem.* **2016**, *85*, 289–301. [CrossRef]
52. Calvo, A.; Angelome, P.C.; Sanchez, V.M.; Scherlis, D.A.; Williams, F.G; Soller-Illia, G.J.A.A. Mesoporous Aminopropyl-Functionalized Hybrid Thin Films with Modulable Surface and Environment-Responsive Behavior. *Chem. Mater.* **2008**, *20*, 4661–4668. [CrossRef]
53. Kim, J.; Seidler, P.; Wan, L.S.; Fill, C. Formation, structure and reactivity of amino-terminated organic films on silicon substrates. *J. Colloid Interface Sci.* **2009**, *329*, 114–119. [CrossRef] [PubMed]
54. Kjellman, T.; Xia, X.; Alfredsson, V.; Garcia-Bennett, A.E. Influence of microporosity in SBA-15 on the release properties of anticancer drug dasatinib. *J. Mater. Chem. B* **2014**, *2*, 5265–5271. [CrossRef]